



Stability Limits of a PD Controller for a Flywheel Supported on Rigid Rotor and Magnetic Bearings

Albert F. Kascak

U.S. Army Research Laboratory, Glenn Research Center, Cleveland, Ohio

Gerald V. Brown

Glenn Research Center, Cleveland, Ohio

Ralph H. Jansen

University of Toledo, Toledo, Ohio

Timothy P. Dever

QSS Group, Inc., Cleveland, Ohio

The NASA STI Program Office . . . in Profile

Since its founding, NASA has been dedicated to the advancement of aeronautics and space science. The NASA Scientific and Technical Information (STI) Program Office plays a key part in helping NASA maintain this important role.

The NASA STI Program Office is operated by Langley Research Center, the Lead Center for NASA's scientific and technical information. The NASA STI Program Office provides access to the NASA STI Database, the largest collection of aeronautical and space science STI in the world. The Program Office is also NASA's institutional mechanism for disseminating the results of its research and development activities. These results are published by NASA in the NASA STI Report Series, which includes the following report types:

- **TECHNICAL PUBLICATION.** Reports of completed research or a major significant phase of research that present the results of NASA programs and include extensive data or theoretical analysis. Includes compilations of significant scientific and technical data and information deemed to be of continuing reference value. NASA's counterpart of peer-reviewed formal professional papers but has less stringent limitations on manuscript length and extent of graphic presentations.
- **TECHNICAL MEMORANDUM.** Scientific and technical findings that are preliminary or of specialized interest, e.g., quick release reports, working papers, and bibliographies that contain minimal annotation. Does not contain extensive analysis.
- **CONTRACTOR REPORT.** Scientific and technical findings by NASA-sponsored contractors and grantees.

- **CONFERENCE PUBLICATION.** Collected papers from scientific and technical conferences, symposia, seminars, or other meetings sponsored or cosponsored by NASA.
- **SPECIAL PUBLICATION.** Scientific, technical, or historical information from NASA programs, projects, and missions, often concerned with subjects having substantial public interest.
- **TECHNICAL TRANSLATION.** English-language translations of foreign scientific and technical material pertinent to NASA's mission.

Specialized services that complement the STI Program Office's diverse offerings include creating custom thesauri, building customized databases, organizing and publishing research results . . . even providing videos.

For more information about the NASA STI Program Office, see the following:

- Access the NASA STI Program Home Page at <http://www.sti.nasa.gov>
- E-mail your question via the Internet to help@sti.nasa.gov
- Fax your question to the NASA Access Help Desk at 301-621-0134
- Telephone the NASA Access Help Desk at 301-621-0390
- Write to:
NASA Access Help Desk
NASA Center for AeroSpace Information
7121 Standard Drive
Hanover, MD 21076



Stability Limits of a PD Controller for a Flywheel Supported on Rigid Rotor and Magnetic Bearings

Albert F. Kascak

U.S. Army Research Laboratory, Glenn Research Center, Cleveland, Ohio

Gerald V. Brown

Glenn Research Center, Cleveland, Ohio

Ralph H. Jansen

University of Toledo, Toledo, Ohio

Timothy P. Dever

QSS Group, Inc., Cleveland, Ohio

Prepared for the

Guidance, Navigation, and Control Conference and Exhibit

sponsored by the American Institute of Aeronautics and Astronautics

San Francisco, California, August 15–18, 2005

National Aeronautics and
Space Administration

Glenn Research Center

This work was sponsored by the Low Emissions Alternative Power Project of the Vehicle Systems Program at the NASA Glenn Research Center.

Available from

NASA Center for Aerospace Information
7121 Standard Drive
Hanover, MD 21076

National Technical Information Service
5285 Port Royal Road
Springfield, VA 22100

Available electronically at <http://gltrs.grc.nasa.gov>

Stability Limits of a PD Controller for a Flywheel Supported on Rigid Rotor and Magnetic Bearings

Albert F. Kascak
U.S. Army Research Laboratory
Glenn Research Center
Cleveland, Ohio 44135

Gerald V. Brown
National Aeronautics and Space Administration
Glenn Research Center
Cleveland, Ohio 44135

Ralph H. Jansen
University of Toledo
Toledo, Ohio 43606

Timothy P. Dever
QSS Group, Inc.
Cleveland, Ohio 44135

Abstract

Active magnetic bearings are used to provide a long-life, low-loss suspension of a high-speed flywheel rotor. This paper describes a modeling effort used to understand the stability boundaries of the PD controller used to control the active magnetic bearings on a high speed test rig. Limits of stability are described in terms of allowable stiffness and damping values which result in stable levitation of the nonrotating rig. Small signal stability limits for the system is defined as a nongrowth in vibration amplitude of a small disturbance. A simple mass-force model was analyzed. The force resulting from the magnetic bearing was linearized to include negative displacement stiffness and a current stiffness. The current stiffness was then used in a PD controller. The phase lag of the control loop was modeled by a simple time delay. The stability limits and the associated vibration frequencies were measured and compared to the theoretical values. The results show a region on stiffness versus damping plot that have the same qualitative tendencies as experimental measurements.

The resulting stability model was then extended to a flywheel system. The rotor dynamics of the flywheel was modeled using a rigid rotor supported on magnetic bearings. The equations of motion were written for the center of mass and a small angle linearization of the rotations about the center of mass. The stability limits and the associated vibration frequencies were found as a function of nondimensional magnetic bearing stiffness and damping and nondimensional parameters of flywheel speed and time delay.

Nomenclature

<i>A</i>	amplitude of oscillation
<i>c</i>	damping coefficient
<i>C</i>	damping coefficient of combined bearings
<i>F</i>	force
<i>I_P</i>	polar moment of inertia
<i>I_T</i>	transverse moment of inertia
<i>k</i>	stiffness coefficient

K	stiffness coefficient of combined bearings
m	modal mass
x	lateral displacement
R	complex lateral displacement
R'	complex rotation about -x and +y-axis
α	real part nondimensional eigenvalue or rotation about y-axis
β	imaginary part nondimensional eigenvalue or rotation about x-axis
η	ratio of polar to transverse moment of inertia
Δt	time delay
$\Delta\phi$	phase change of transfer function
$\Delta\omega$	change of frequency
ω	circular frequency
λ	eigenvalue
μ	nondimensional eigenvalue
τ	nondimensional time
ζ	damping ratio

Subscripts

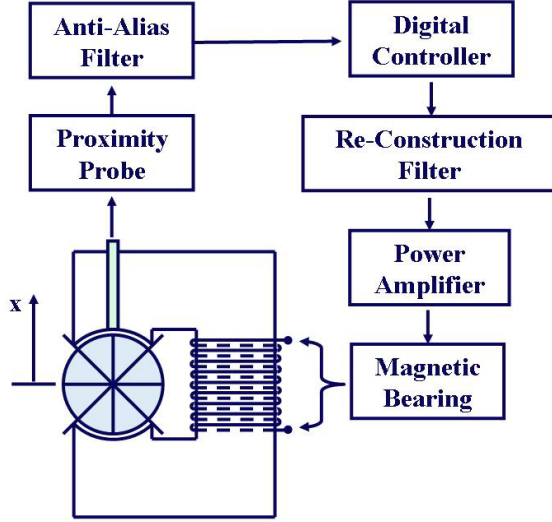
n	negative stiffness
p	proportional
d	derivative
0	un-damp natural frequency

Introduction

High speed flywheel systems are being developed at the NASA Glenn Research Center (NASA Glenn) in Cleveland, Ohio. Flywheels show promise as an alternative to batteries and reaction wheels for space systems. Strengths of this technology include high energy density, long life, capability for up to 90 percent depth of discharge, and peaking or pulse power capability. Flywheels can also be deployed in an array which provides both energy storage and attitude control. A system level flywheel test bed called the High Energy Flywheel Facility (HEFF) is operational at NASA Glenn, which includes two high-speed flywheel modules.

The system level flywheel test bed consists of a rotating carbon fiber ring supported on a hub with a shaft. The flywheel modules use a motor/generator coaxial with the rotor to facilitate energy storage and retrieval. The shaft is supported on two noncontacting magnetic bearings. One of the bearings gives both a radial and axial support. The system utilizes a feedback loop in which the position of the rotor is measured with eddy current sensors and used as the input to the magnetic bearing control algorithm.

The magnetic bearing system uses magnetic forces to levitate the shaft between opposing magnetic poles (Fig. 1). The rotor is attracted to one pole or the other pole and is inherently unstable. The magnetic bearing system is stabilized with an active control system. The magnetic bearing control system for a flywheel measures the location of the rotor with eddy current proximity sensors. The signal is low pass filtered with an anti-alias filter. The signal is digitized and sent to a computer which applies a control algorithm, (digital controller). The digital signal is then converted to an analog signal and sent to a low pass re-construction filter. This signal commands the power amplifiers, which produce current in the magnetic bearing coils. This magnetic bearing actuator produces forces which stably suspend the rotor between the opposite magnetic poles.



Magnetic Bearing and Control System

Figure 1.—Shows the magnetic bearing system: proximity sensor, anti-alias filter, digital controller, re-construction filter, power amplifier, magnetic bearing actuator.

Several groups have developed magnetic bearing controllers for high speed flywheel systems. Many different approaches have been used, varying from PID to modal or adaptive methods. The controller complexity depends on the details of the flywheel mechanical design and the performance requirements. Pichot (Ref. 1) discusses the benefits of a notch filter based controller in comparison to a PID control for a large flywheel. Tsiotras has used an H infinity and variable bias controllers for small flywheel and gyroscope systems (Refs. 2 and 3). Dr. Alan Palazollo at Texas A&M developed a modal control system which was applied to a 60,000 rpm flywheel (Ref. 4). At NASA Glenn this approach has been refined and is discussed in a paper by Dever (Ref. 5).

Each of the components involved in the magnetic bearing and control system has a time delay associated with the components. For the analog devices, they are approximated by a linear time delay low pass filter. The amplitude of the transfer function is assumed to be a constant and the phase is linear. The time delay is the change in phase of the transfer function divided by the change in frequency. For the digital devices this time delay is the loop time for each measurement. The total time delay is the sum of the individual time delays.

$$\begin{aligned} \Delta t_{\text{analog-device}} &= \Delta\phi_{\text{analog-device}} / \Delta\omega \\ \Delta t &= \Delta t_{\text{prox}} + \Delta t_{\text{alias}} + \Delta t_{\text{control}} + \Delta t_{\text{recon}} + \Delta t_{\text{amp}} + \Delta t_{\text{mag}} \end{aligned} \quad (1)$$

The magnetic bearing and controller have other requirements beside stability. Another requirement is its response to transients. To improve the magnetic bearing's transient response a bias magnetic field is applied. The source of this field is a permanent magnet placed in the magnetic circuit of the bearing. The result of this bias field causes the rotor to behave as though it was supported on a spring with a negative stiffness. There is no time delay associated with the bias field since it is caused by a permanent magnet. This paper describes a modeling effort which was used to theoretically map the stability boundaries of the magnetic bearing controller which levitates the high speed flywheel rotor. The controller analyzed is a P-D controller which causes the magnetic bearing to produce two forces. The first force is proportional to the displacement and the second force is proportional to the derivative of the displacement, the velocity.

Discussion of Test Rig Stability Data

Tests were performed on a high speed shaft rig to determine the region of stable operation. A high speed shaft rig was used in place of the actual flywheel rig. This rig was simpler, easier to operate, and analyze than the actual flywheel rig. The high speed shaft rig was simply a shaft supported on two magnetic bearings (Fig. 2). A simple plant model was used as an estimator for the velocity and displacement, and the difference between the measured and estimated displacement was used for control. The shaft was not rotating. Similar test were performed on each bearing, (one at a time), and in a given lateral direction. For a given proportional gain, the derivative gain was varied noting the region of stable operation and the frequencies of vibration at the boundaries.

The measured results for the lower and upper magnetic bearing are shown in Figures 3 and 4. Both bearings have similar shaped regions of stability, but the numerical values are different because the bearings are different. The region of stable operation is limited at small proportional gains by the gain necessary to cancel the negative stiffness. If the negative stiffness is not exceeded by the proportion stiffness, the rotor will just go to one pole or the other, (static instability). At high proportional gains there is no stable region of operation. At intermediate proportional gains there is a stable region between two derivative gains. Intuitively one might expect that a minimum amount of damping is necessary for stability, but why would one expect that a large amount of damping would cause instability?

Intuitively one might expect the proportional gain to be parabolic with respect to the frequency, ($\omega^2 = K/M$). This seems to be true at low frequencies, (the lower curve on the stability plot), but is not true for the higher frequencies, (the upper curve on the stability plot). The derivative gain seems to be parabolic with respect to the frequency. For a mass-stiffness-damped system any damping would result in a damped oscillation, not a stable oscillation.

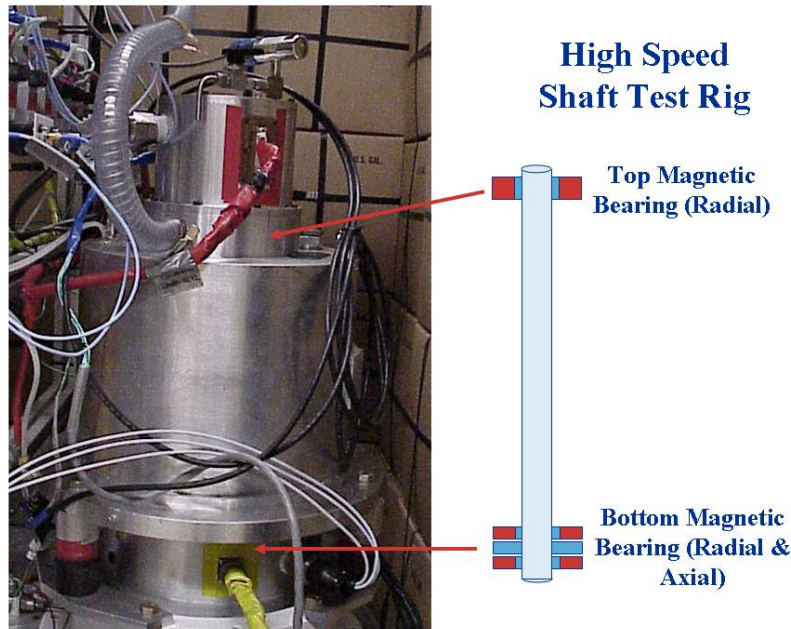


Figure 2.—Shows the High Speed Shaft Rig use to test magnetic bearing control systems to be used on the Energy Storage Flywheel.

Stability Limits & Oscillation Frequency of Bottom Magnetic Bearing

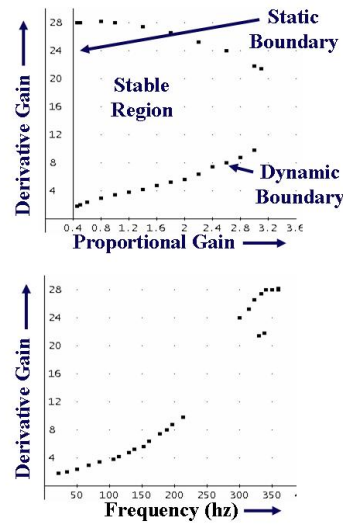
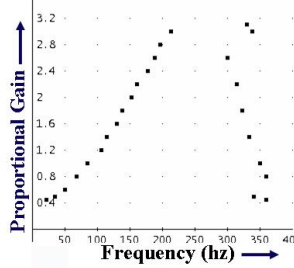


Figure 3.—Shows the stability data for the bottom magnetic bearing. The top magnet bearing's parameters were held constant.

Stability Limits & Oscillation Frequency of Top Magnetic Bearing

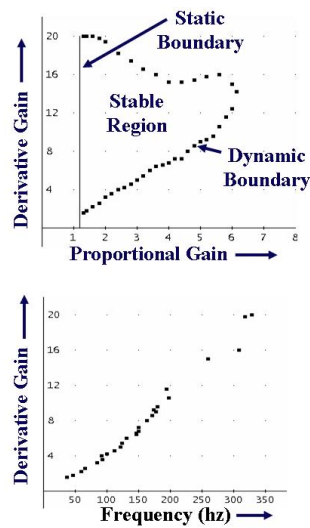
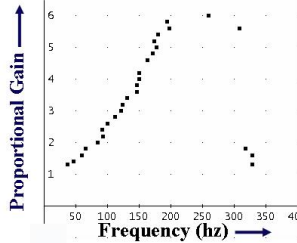


Figure 4.—Shows the stability data for the top magnetic bearing. The bottom magnetic bearing's parameters were held constant.

Test Rig Stability Analysis

A simple model of the high speed shaft rig is a modal mass of the shaft being accelerated by a radial force produced by the magnetic bearing. The equation of motion is then:

$$m\ddot{x}(t) = F_{mag} = k_n x(t) - c\dot{x}(t - \Delta t) - kx(t - \Delta t) \quad (2)$$

The force produced by the magnetic bearing has a negative stiffness term associated with the permanent magnet bias field; and, stiffness and damping terms produced by the magnetic bearing controller. The controller terms have a time delay associated with the various components in the control loop. The classical small signal stability analysis assumes an eigenvalue solution of the form:

$$x(t) = Ae^{\lambda t} \Rightarrow x(t - \Delta t) = x(t)e^{-\lambda \Delta t} \quad (3)$$

Substituting this solution into the equation of motion yields:

$$0 = m\lambda^2 - k_n + c\lambda e^{-\lambda \Delta t} + ke^{-\lambda \Delta t} \quad (4)$$

If the following nondimensional parameters are defined:

$$\begin{aligned} \mu &= \lambda \Delta t \\ \tau_0^2 &= k \Delta t^2 / m \\ 2\zeta\tau_0 &= c \Delta t / m \\ \tau_n^2 &= k_n \Delta t^2 / m \end{aligned} \quad (5)$$

Then the eigenvalue equation becomes:

$$0 = \mu^2 - \tau_n^2 + 2\zeta\tau_0\mu e^{-\mu} + \tau_0^2 e^{-\mu} \quad (6)$$

The eigenvalue equation has two solutions depending on whether the eigenvalue μ is real or complex. If the eigenvalue is real, the nondimensional stiffness becomes:

$$\mu = \alpha (\text{Re } al) \Rightarrow \tau_0^2 = -(\alpha^2 - \tau_n^2) e^\alpha - 2\zeta\tau_0\alpha \quad (7)$$

If the eigenvalue is complex, then the imaginary portion of the eigenvalue is the circular frequency of the vibration times the time delay:

$$\mu = \alpha + i\beta \Rightarrow \beta = \omega_c \Delta t \quad (8)$$

Solving the real and imaginary portions of the eigenvalue equation, the nondimensional damping becomes:

$$2\zeta\tau_0 = -\text{Im}\left((\mu^2 - \tau_n^2)e^\mu\right) / \beta \quad (9)$$

And the nondimensional stiffness becomes:

$$\tau_0^2 = -\text{Re}\left((\mu^2 - \tau_n^2)e^\mu\right) + (\alpha/\beta)\text{Im}\left((\mu^2 - \tau_n^2)e^\mu\right) \quad (10)$$

If the real part of the eigenvalue α is positive, the vibrations grow in time and the system is unstable. If α is negative, the vibrations decay in time and the system is stable. α equal to zero defines the stability boundary.

$$\begin{aligned}\alpha = 0 \Rightarrow \mu &= i\beta \\ 2\zeta\tau_0 &= (\beta^2 + \tau_n^2) \sin(\beta)/\beta \\ \tau_0^2 &= (\beta^2 + \tau_n^2) \cos(\beta)\end{aligned}\quad (11)$$

The stiffness and damping are defined in term of the proportional and derivative gains of the controller:

$$\begin{aligned}k &= k_p G_p \\ c &= c_d G_d\end{aligned}\quad (12)$$

The nondimensional stiffness and damping are related to the proportional and derivative gains by

$$\begin{aligned}\tau_0^2 &= \tau_p^2 G_p \\ 2\zeta\tau_0 &= \tau_d G_d\end{aligned}\quad (13)$$

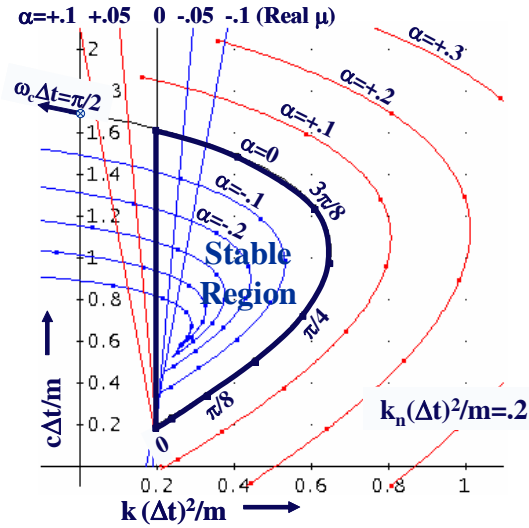
Correlation of Test Rig Data

A simple model of the high speed shaft rig is a modal mass of the shaft being accelerated by a radial force produced by the magnetic bearing. The force produced by the magnetic bearing has a negative stiffness term associated with the permanent magnet bias field; and, stiffness and damping terms produced by the magnetic bearing controller. The controller terms have a time delay associated with the various components in the control loop. The classical small signal stability analysis assumes an eigenvalue solution of the equation of motion. This solution can be nondimensional by defining time constants which are the product of various frequencies associated with the negative stiffness, proportional stiffness, and the eigenvalue multiplied by the time delay.

Figure 5 shows the stable region for a magnetic bearing with time delay. It also shows the growth rate, α (real part of the eigenvalue), for both the static, and dynamic stability, and the frequency of oscillations, β (imaginary part of the eigenvalue), for dynamic stability. The nondimensional stiffness for the static stability analysis is given by Equation (7), and for the dynamic stability analysis is given by Equation (10). The nondimensional damping for the static stability analysis is an independent variable, and for the dynamic stability analysis is given by Equation (9). For both the static and dynamic stability analysis, if the real part of the eigenvalue α is defined positive, the vibrations grow in time and the system is unstable. If α is defined negative, the vibrations decay in time and the system is stable. α equal to zero defines the stability boundary. The absolute value of the imaginary part of the eigenvalue, β , is a parameter which varies from 0 to $\pi/2$. A nondimensional negative stiffness of 0.2 was assumed.

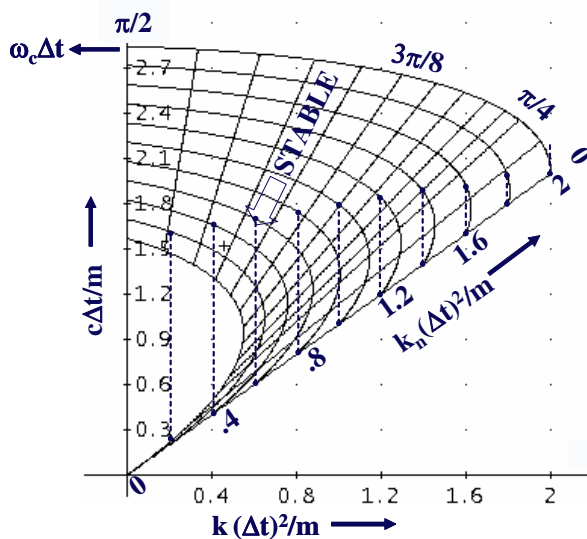
Figure 5 shows a plot of the nondimensional damping versus nondimensional stiffness for various growth rates. The nondimensional stiffness and nondimensional damping are related to the proportional and derivative gains (Eq. (13)). Figure 5 shows a stable region similar to that shown in Figures 3 and 4.

Figure 6 shows the dynamic stability map for a magnetic bearing with time delay for various negative stiffness, K_n . The solid lines represent dynamic stability limits and the dotted lines represent the static stability limits. For both cases, α (real part of the eigenvalue) equal to zero. There is a stable region for nondimensional negative stiffness, nondimensional stiffness, and nondimensional damping between 0 and 2. The nondimensional stiffness and nondimensional damping have to be greater than the nondimensional negative stiffness.



Growth Rate of Disturbance of PD Controlled (Magnetic Bearing with Time Delay)

Figure 5.—Shows the stable region for a magnetic bearing with time delay. It also shows the growth rate, α (real part of the eigenvalue), for both the static and dynamic stability, and the frequency of oscillations, β (imaginary part of the eigenvalue) for dynamic stability.



Stability Map of PD Controlled (Magnetic Bearing with Time Delay)

Figure 6.—Shows the dynamic stability map for a magnetic bearing with time delay for various negative stiffness, K_n . The dotted line represents the static stability limit.

Figure 7 shows the correlation of stability data for the bottom magnetic bearing shown on Figure 3. Figure 8 shows the correlation of stability data for the top magnetic bearing shown on Figure 4. The data shown on Figures 3 and 4 were correlated with different proportionality coefficients (Eq. (13)), for the proportional and derivative gain for each magnetic bearing. (The top magnetic bearing actuator was different than the bottom. The top magnetic bearing actuator could only apply a radial force and the bottom magnetic bearing actuator could apply both a radial and axial force.) There was only one digital controller for both bearings and the rest of the control system components were identical so the same time delay was used for both magnetic bearings. The time delay was calculated from the zero crossing frequency of the proportional gain, ($2\pi f_c \Delta t = \pi/2$). The nondimensional negative stiffness for the top magnetic bearing was $0.99 \times 1.2 = 1.19$, and for the bottom magnetic bearing was $0.155 \times 0.4 = 0.062$. The correlation showed a stable region on derivative gain versus proportional gain plot that have the same qualitative tendencies as experimental measurements. In general the correlation of the proportional gain and derivative gain with the oscillation frequency at the stability boundary was very good.

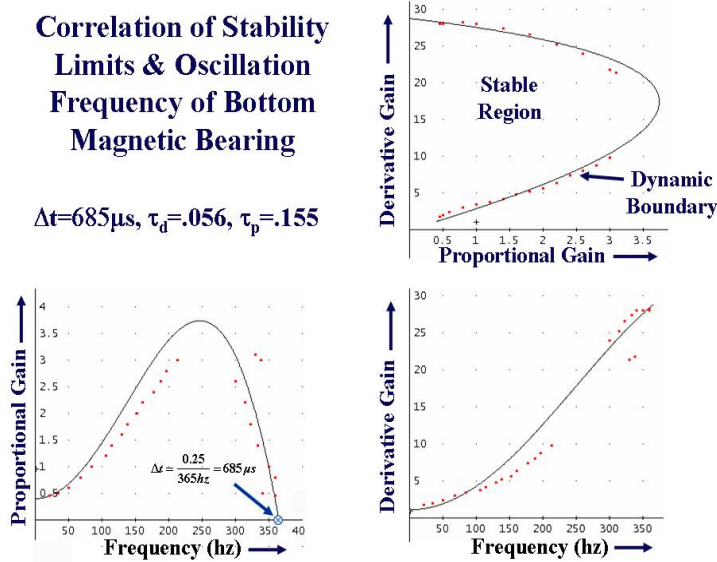


Figure 7.—Shows the correlation of stability data for the bottom magnetic bearing.

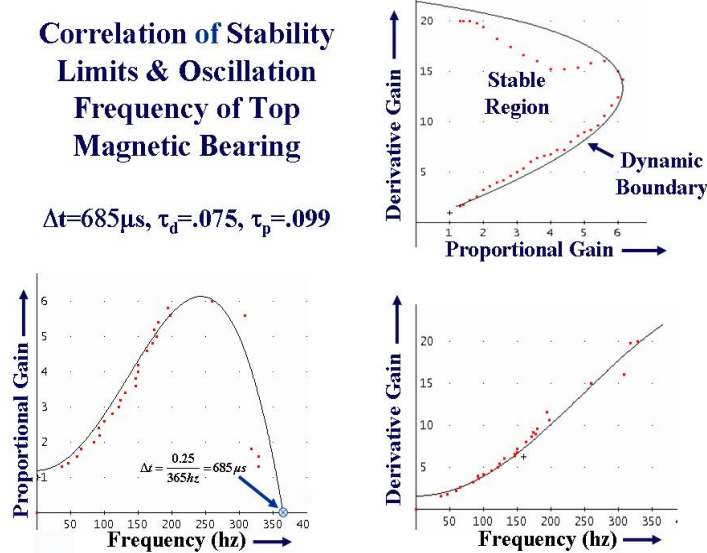


Figure 8.—Shows the correlation of stability data for the top magnetic bearing.

Flywheel Stability Analysis

Figure 9 shows the rigid body rotordynamic model of a flywheel. The rotordynamics of the flywheel can be described in terms of the motion of the center of mass and rotations about the center of mass (Ref. 6). For small displacements the lateral motion is uncoupled from the axial motion. The lateral equations of motion of the center of mass are:

$$\begin{aligned} m\ddot{X}_{cm} &= F_{x1} + F_{x2} \\ m\ddot{Y}_{cm} &= F_{y1} + F_{y2} \end{aligned} \quad (14)$$

For small rotations, the equations of angular motion about the center of mass are:

$$\begin{aligned} I_T\ddot{\beta} + \omega I_P \dot{\alpha} &= L_1 F_{y1} - L_2 F_{y2} \\ I_T\ddot{\alpha} - \omega I_P \dot{\beta} &= L_2 F_{x2} - L_1 F_{x1} \end{aligned} \quad (15)$$

If the x-direction is real and the y-direction is imaginary, then the complex displacement, rotation, and force can be defined as:

$$\begin{aligned} R_{cm} &= X_{cm} + iY_{cm} \\ R' &= \alpha - i\beta \\ F &= F_x + iF_y \end{aligned} \quad (16)$$

The equations of motion become:

$$\begin{aligned} \sum F &= F_2 + F_1 \\ m\ddot{R}_{cm} &= \sum F \\ \sum T &= L_2 F_2 - L_1 F_1 \\ I_T \ddot{R}' - i\omega I_P \dot{R}' &= \sum T \end{aligned} \quad (17)$$

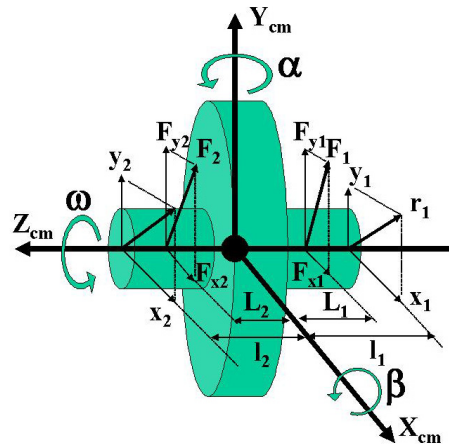


Figure 9.—Shows the rigid body rotordynamic model of a flywheel. The rotordynamics of the flywheel can be described in terms of the motion of the center of mass and rotations about the center of mass.

For a centralized controller the summation of the forces of the magnetic bearings can be expressed as a function of the position and velocity of the center of mass. The summation of the torques about the center of mass can be expressed as a function of the angular position and angular velocity about the center of mass. For a centralized PD controller, (including the negative stiffness), the summation of the force and torque are:

$$\begin{aligned}\sum F &= K_n R_{cm} - KR_{cm} - C\dot{R}_{cm} \\ \sum T &= K'_n R'_{cm} - K'R'_{cm} - C\dot{R}'_{cm}\end{aligned}\quad (18)$$

The centralized controller decoupled the motion of the center of mass and the rotation about the center of mass. If a time delay is included in the controller the equations of motion become:

$$\begin{aligned}m\ddot{R}_{cm}(t) &= K_n R_{cm}(t) - KR_{cm}(t-\Delta t) - C\dot{R}_{cm}(t-\Delta t) \\ I_T \ddot{R}'(t) - i\omega I_P \dot{R}'(t) &= K'_n R'(t) - K'R'(t-\Delta t) - C\dot{R}'(t-\Delta t)\end{aligned}\quad (19)$$

The solution for the motion of the center of mass and that for the rotation about the center of mass is of the same form, if the shaft speed ω is set equal to zero. The solution for the motion of the center of mass is similar to the previous solution presented in the rig analysis. Therefore only motion of the rotation about the center of mass will be solved. If the eigenvalue solution is assumed to be:

$$R'(t) = Ae^{\lambda t} \quad (20)$$

Then the equation of motion becomes:

$$I_T \lambda^2 - i\omega I_P \lambda - K'_n + C'\lambda e^{-\lambda \Delta t} + K'e^{-\lambda \Delta t} = 0 \quad (21)$$

If the following nondimensional parameters are defined:

$$\begin{aligned}\mu &= \lambda \Delta t \\ \tau_0^2 &= k \Delta t^2 / I_T \\ 2\zeta\tau_0 &= c \Delta t / I_T \\ \tau_n^2 &= k_n \Delta t^2 / I_T \\ \tau\eta &= \omega \Delta t I_P / I_T\end{aligned}\quad (22)$$

Then the eigenvalue equation becomes:

$$0 = (\mu^2 - i\tau\eta\mu - \tau_n^2) e^\mu + 2\zeta\tau_0\mu + \tau_0^2 \quad (23)$$

The eigenvalue equation does not have a real solution unless ω is zero. If the eigenvalue is complex, then the imaginary portion of the eigenvalue is the circular frequency of the vibration times the time delay:

$$\mu = \alpha + i\beta \Rightarrow \beta = \omega_c \Delta t \quad (24)$$

Solving the real and imaginary portions of the eigenvalue equation, the nondimensional damping becomes:

$$2\zeta\tau_0 = -\text{Im}\left(\left(\mu^2 - i\tau\eta\mu - \tau_n^2\right)e^\mu\right)/\beta \quad (25)$$

And the nondimensional stiffness becomes:

$$\tau_0^2 = -\text{Re}\left(\left(\mu^2 - i\tau\eta\mu - \tau_n^2\right)e^\mu\right) + (\alpha/\beta)\text{Im}\left(\left(\mu^2 - i\tau\eta\mu - \tau_n^2\right)e^\mu\right) \quad (26)$$

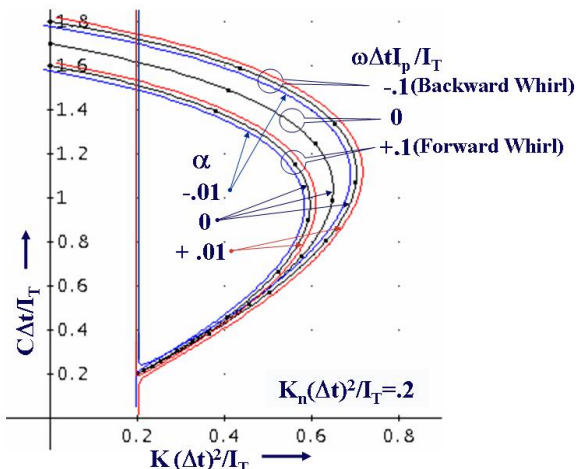
If the real part of the eigenvalue α is positive, the vibrations grow in time and the system is unstable. If α is negative, the vibrations decay in time and the system is stable. α equal to zero defines the stability boundary. Equation (27) defines the nondimensional damping and stiffness at the transition between stable and unstable operation of the flywheel.

$$\begin{aligned} \alpha = 0 &\Rightarrow \mu = i\beta \\ 2\zeta\tau_0 &= \left(\beta^2 - \tau\eta\beta + \tau_n^2\right)\sin(\beta)/\beta \\ \tau_0^2 &= \left(\beta^2 - \tau\eta\beta + \tau_n^2\right)\cos(\beta) \end{aligned} \quad (27)$$

Discussion of Results

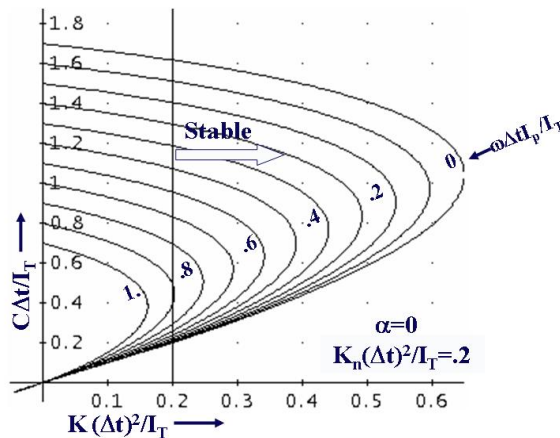
A simple model of the flywheel is shown in Figure 9. The rotordynamics of the flywheel can be described in terms of the motion of the center of mass and rotations about the center of mass (Ref. 6). For small displacements the lateral motion is uncoupled from the axial motion. The rotor center of mass is being accelerated by radial forces produced by the magnetic bearings. The rotation of the rotor about the center of mass is being accelerated by the torques produced by the radial forces of the magnetic bearings. The forces produced by the magnetic bearings have a negative stiffness term associated with the permanent magnet bias fields; and a stiffness and damping terms produced by the magnetic bearing controller. A centralized controller decouples the motion of the center of mass and the rotation about the center of mass. The controller terms have a time delay associated with the various components in the control loop. The classical small signal stability analysis assumes an eigenvalue solution of the equation of motion. This solution can be nondimensional by defining time constants which are the product of various frequencies associated with the negative stiffness, proportional stiffness, rotational speed, and the eigenvalue multiplied by the time delay. The nondimensional equations for the motion of the center of mass are of the same form as the nondimensional equations for the motion of rotation about the center of mass at zero rotational speed. These equations were solved in the previous section, and only the rotation equations about the center of mass will be solved.

Figure 10 shows the stable region for a rigid flywheel supported on magnetic bearings using a centralized controller with time delay. Gyroscopic effects result in either a forward or backward whirl. It also shows the growth rate, α (real part of the eigenvalue), and the frequency of oscillations, β (imaginary part of the eigenvalue). The nondimensional stiffness is given by Equation (26) and the nondimensional damping is given by Equation (24). If the real part of the eigenvalue α is defined positive, the vibrations grow in time and the system is unstable. If α is defined negative, the vibrations decay in time and the system is stable. α equal to zero defines the stability boundary. The imaginary part of the eigenvalue, β , is a parameter which varies from 0 to $+\pi/2$. The nondimensional speed of the flywheel was +0.1 for forward whirl, 0 for nonrotation, and -0.1 for backward whirl. A nondimensional negative stiffness of 0.2 was assumed.



**Growth Rate of Disturbance of PD Controlled
(Gyroscopic Effects & Magnetic Bearing with Time Delay)**

Figure 10.—Shows the stable region for a rigid flywheel supported on magnetic bearings using a centralized controller with time delay. Gyroscopic effects result in either a forward or backward whirl. If the growth rate, α (real part of the eigenvalue), is less than zero the system is stable.

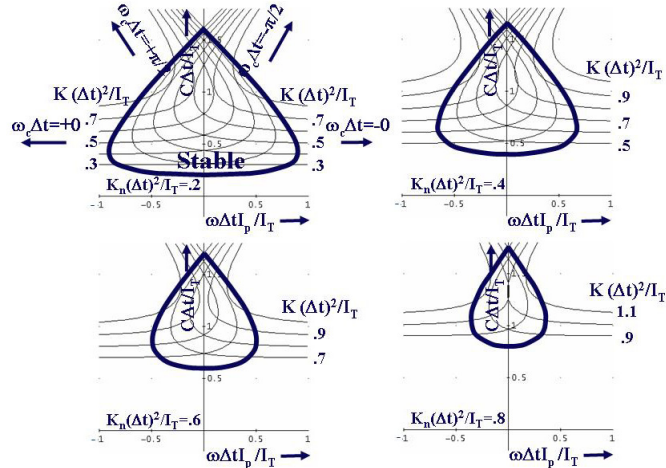


**Stability Map of Disturbance of PD Controlled
(Gyroscopic Effects & Magnetic Bearing with Time Delay)**

Figure 11.—Shows the dynamic stability map for a flywheel supported on magnetic bearings with time delay for various values of speed, ω . The stiffness must be greater than the negative stiffness for the system to be stable.

Figure 10 shows a plot of the nondimensional damping versus nondimensional stiffness for various growth rates. Figure 10 shows a stable region similar to that shown in Figure 5 except it is now limited by the forward whirl. The stable region is smaller than that for the nonrotating rotor.

Figure 11 shows the dynamic stability map for a flywheel supported on magnetic bearings with time delay for various values of speed, ω . The stiffness must be greater than the negative stiffness for the system to be stable. To the left of the solid lines represent stability limits resulting from the forward whirl. (The real part of the eigenvalue, α , equals zero.) The stable region becomes smaller for higher nondimensional rotor speeds. There is no stable region for nondimensional rotor speeds higher than 0.8.



**Stability Speed Limits of PD Controlled
(Gyroscopic Effects & Magnetic Bearing with Time Delay)**

Figure 12.—Shows the dynamic stability map for a flywheel supported on magnetic bearings with time delay for various values of negative stiffness, K_n . It shows plots of nondimensional damping versus nondimensional flywheel speed. It shows both forward and backward whirl, and the stable region is between the forward and backward whirl for the appropriate stiffness. The stiffness must be greater than the negative stiffness for the system to be stable.

Figure 12 shows the dynamic stability map for a flywheel supported on magnetic bearings with time delay for various values of negative stiffness, K_n . It shows plots of nondimensional damping versus nondimensional flywheel speed. It shows both forward and backward whirl, and the stable region is between the forward and backward whirl for the appropriate stiffness. The stiffness must be greater than the negative stiffness for the system to be stable. As the system negative stiffness increases the stable region decreases and the maximum flywheel speed decreases.

Conclusion

Active magnetic bearings are used to provide a long-life, low-loss suspension of a high-speed flywheel rotor. This paper describes a modeling effort used to understand the stability boundaries of the PD controller used to control the active magnetic bearings. Limits of stable levitation and associated vibration frequencies were measured for a nonrotating rotor in terms of allowable stiffness and damping values. The following conclusions were made:

1. These results could be correlated by a simple time delay model used for the active magnetic bearing controller.
2. The time delay could be calculated from the zero crossing frequency of the proportional gain.
3. The product of the frequency of vibration times the delay time varied between 0 and $\pi/2$.

The analysis was extended to a rotating rigid flywheel supported on active magnetic bearings. The following conclusions were made:

1. The larger the negative stiffness, the smaller the region of stability.
2. The larger the speed, the smaller the region of stability.
3. The forward whirl limited the region of stability

The results of this modeling effort showed a region (on damping versus stiffness), plot that has the same qualitative tendencies as experimental measurements and the analysis could be extended to more complicated cases including gyroscopic effects.

References

1. M.A. Pichot, et al., "Active Magnetic Bearings for Energy Storage Systems for Combat Vehicles," IEEE Transactions on Magnetics, Vol. 37, No. 1, January 2001.
2. P. Tsiotras, S. Mason, "Self Scheduled H_∞ Controllers for Magnetic Bearings," University of Virginia, Charlottesville, VA.
3. P. Tsiotras, M. Arcak, "Low-Bias Control of AMB Subject to Voltage Saturation: State-Feedback and Observer Designs," IEEE, 2005.
4. "System and Method for Controlling Suspension Using a Magnetic Field," U.S. Patent: (US 6,323,614B1); Date of Patent: Nov. 27, 2001; Inventors: Palazzolo, A., Mu Li, Uhn Joo Na, Erwin Thomas.
5. T. Dever, et al., "Modeling and Development of a Magnetic Bearing Controller for a High Speed Flywheel System," IECEC, 2004.
6. "Rotordynamics of Turbomachinery," Dr. John M. Vance, Texas A&M, Wiley-Interscience Publication, pp. 121–122.

REPORT DOCUMENTATION PAGE			<i>Form Approved OMB No. 0704-0188</i>
Public reporting burden for this collection of information is estimated to average 1 hour per response, including the time for reviewing instructions, searching existing data sources, gathering and maintaining the data needed, and completing and reviewing the collection of information. Send comments regarding this burden estimate or any other aspect of this collection of information, including suggestions for reducing this burden, to Washington Headquarters Services, Directorate for Information Operations and Reports, 1215 Jefferson Davis Highway, Suite 1204, Arlington, VA 22202-4302, and to the Office of Management and Budget, Paperwork Reduction Project (0704-0188), Washington, DC 20503.			
1. AGENCY USE ONLY (Leave blank)	2. REPORT DATE	3. REPORT TYPE AND DATES COVERED	
	January 2006	Technical Memorandum	
4. TITLE AND SUBTITLE		5. FUNDING NUMBERS	
Stability Limits of a PD Controller for a Flywheel Supported on Rigid Rotor and Magnetic Bearings		WBS-22-066-30-02 1L161102AF20	
6. AUTHOR(S)		7. PERFORMING ORGANIZATION NAME(S) AND ADDRESS(ES)	
Albert F. Kascak, Gerald V. Brown, Ralph H. Jansen, and Timothy P. Dever		National Aeronautics and Space Administration John H. Glenn Research Center at Lewis Field Cleveland, Ohio 44135-3191	
8. PERFORMING ORGANIZATION REPORT NUMBER		9. SPONSORING/MONITORING AGENCY NAME(S) AND ADDRESS(ES)	
E-15301		National Aeronautics and Space Administration Washington, DC 20546-0001 and U.S. Army Research Laboratory Adelphi, Maryland 20783-1145	
10. SPONSORING/MONITORING AGENCY REPORT NUMBER		11. SUPPLEMENTARY NOTES	
NASA TM-2006-213979 ARL-TR-3745 AIAA-2005-5956		Prepared for the Guidance, Navigation, and Control Conference and Exhibit sponsored by the American Institute of Aeronautics and Astronautics, San Francisco, California, August 15-18, 2005. Albert F. Kascak, e-mail: Albert.F.Kascak@grc.nasa.gov, U.S. Army Research Laboratory, NASA Glenn Research Center; Gerald V. Brown, e-mail: Gerald.V.Brown@grc.nasa.gov, NASA Glenn Research Center; Ralph H. Jansen, e-mail: Ralph.H.Jansen@grc.nasa.gov, University of Toledo, 2801 W. Bancroft Street, Toledo, Ohio 43606-3390; and Timothy P. Dever, e-mail: Timothy.P.Deve@grc.nasa.gov, QSS Group, Inc., 21000 Brookpark Road, Cleveland, Ohio 44135. Responsible person, Albert F. Kascak, organization code RSS, 216-433-6024.	
12a. DISTRIBUTION/AVAILABILITY STATEMENT		12b. DISTRIBUTION CODE	
Unclassified - Unlimited Subject Category: 37 Available electronically at http://gltrs.grc.nasa.gov This publication is available from the NASA Center for AeroSpace Information, 301-621-0390.			
13. ABSTRACT (Maximum 200 words)			
Active magnetic bearings are used to provide a long-life, low-loss suspension of a high-speed flywheel rotor. This paper describes a modeling effort used to understand the stability boundaries of the PD controller used to control the active magnetic bearings on a high speed test rig. Limits of stability are described in terms of allowable stiffness and damping values which result in stable levitation of the nonrotating rig. Small signal stability limits for the system is defined as a nongrowth in vibration amplitude of a small disturbance. A simple mass-force model was analyzed. The force resulting from the magnetic bearing was linearized to include negative displacement stiffness and a current stiffness. The current stiffness was then used in a PD controller. The phase lag of the control loop was modeled by a simple time delay. The stability limits and the associated vibration frequencies were measured and compared to the theoretical values. The results show a region on stiffness versus damping plot that have the same qualitative tendencies as experimental measurements. The resulting stability model was then extended to a flywheel system. The rotor dynamics of the flywheel was modeled using a rigid rotor supported on magnetic bearings. The equations of motion were written for the center of mass and a small angle linearization of the rotations about the center of mass. The stability limits and the associated vibration frequencies were found as a function of nondimensional magnetic bearing stiffness and damping and nondimensional parameters of flywheel speed and time delay.			
14. SUBJECT TERMS			15. NUMBER OF PAGES
Flywheels; Magnetic bearings; Gyroscopic; Energy storage			21
			16. PRICE CODE
17. SECURITY CLASSIFICATION OF REPORT	18. SECURITY CLASSIFICATION OF THIS PAGE	19. SECURITY CLASSIFICATION OF ABSTRACT	20. LIMITATION OF ABSTRACT
Unclassified	Unclassified	Unclassified	

